*Graphical Abstract

Lead on high temperature rice straw biochars is generally more stable

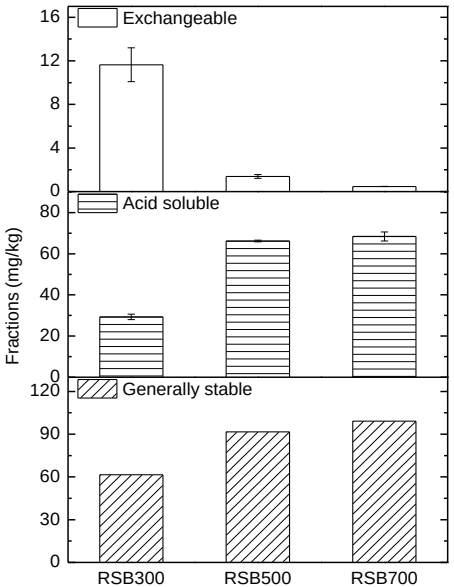

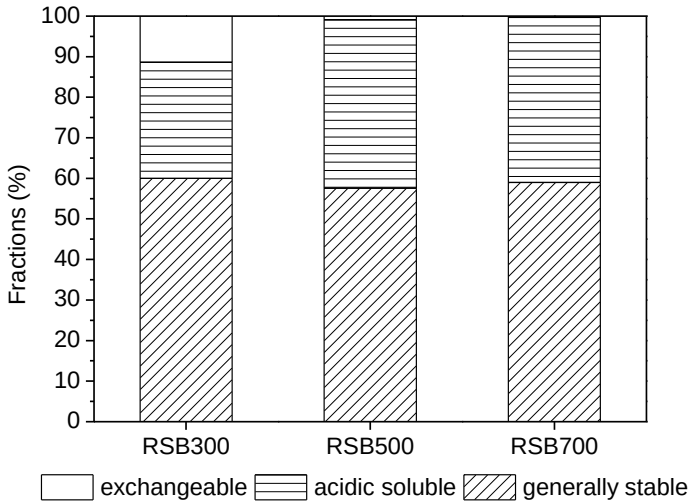

***Highlights (for review : 3 to 5 bullet points (maximum 85 characters including spaces per bullet point)**

- Higher temperature biochars remove Pb faster and have higher removal capacity
- Precipitation was a mechanism by which all three biochars immobilized Pb
- RSB300 has 11.34% of total immobilized Pb attributed to the exchangeable fraction
- Exchangeable Pb was less than 1% on RSB500 and RSB700
- High temperature rice straw biochars may be more suitable for soil remediation

Effect of production temperature on lead removal mechanisms by rice straw biochars

Zhengtao Shen [1,2,3], Deyi Hou [1,2,*], Fei Jin [4], Junxian Shi [5], Xiaoliang Fan [5], Daniel C.W. Tsang [6], Daniel S. Alessi [3]

1 National Engineering Laboratory for Site Remediation Technologies, Beijing 100015, China

2 School of Environment, Tsinghua University, Beijing 100084, China

3 Department of Earth and Atmospheric Sciences, University of Alberta, Edmonton T6G 2E3, Canada

4 School of Engineering, University of Glasgow, Glasgow G12 8QQ, UK

5 School of Ecology and Environment, Inner Mongolia University, Hohhot 010021, China

6 Department of Civil and Environmental Engineering, Hong Kong Polytechnic University, Hung Hom, Kowloon, Hong Kong, China

*Corresponding author: Deyi Hou, E-mail: houdeyi@tsinghua.edu.cn

Abstract: Production temperature significantly affects biochar properties and consequently the removal mechanisms of heavy metals. In this study, rice straw biochars were produced at 300, 500 and 700 °C (RSB300, RSB500 and RSB700). The influence of production temperature on the adsorption characteristics and removal mechanisms of lead on this set of rice straw biochars were investigated by batch adsorption tests, micro-structural analyses and sequential metal extractions. Biochars produced at higher temperatures had significantly higher pH values and surface areas, resulting in higher metal removal capacities and faster uptake kinetics. Precipitation was a key mechanism for lead removal from solution for all biochars: lead oxalate was precipitated on RSB300, and hydrocerussite was precipitated on RSB500 and RSB700. The immobilized lead fraction on the biochars could be divided into exchangeable, acid soluble and non-available fractions. RSB300 had 11.34% of the total immobilized Pb attributed to the exchangeable fraction, whereas for RSB500 and RSB700, it was less than 1%. Immobilized Pb on RSB500 and RSB700 was almost exclusively attributable to the acid soluble and non-available fractions (>99%). Based on our results, RSB500 and RSB700 are likely much more appropriate for soil remediation of Pb as compared with RSB300.

Keywords: soil remediation, biochar, lead immobilization, adsorption, precipitation, production temperature

1 Introduction

Soil contamination is becoming an increasing threat to human health in China. Polluted agricultural land (19% of total sampling points in China's national soil survey) may produce crops with elevated heavy metals concentrations, which may enter into the human body through ingestion and ultimately damage organ systems (Zhao et al., 2015; Hou and Li, 2017). For these reasons, there is an urgent need to seek effective and sustainable technologies to remediate contaminated agricultural land (Hou and Al-Tabbaa, 2014). Biochar is regarded as a promising material that can reduce the bioavailability/mobility of heavy metals after its addition into contaminated soils (Sohi, 2012). In addition, biochar amendment can promote soil fertility and enhance crop yields, which promotes its use as a green and sustainable remediation material (Hou et al., 2017a; Zhao et al., 2017).

Extensive studies have been carried out recently, to investigate the potential application of biochar in remediation of heavy metal contaminated soils (O'Connor et al., 2018b). Biochar reduces the bioavailability/mobility of heavy metals in soils through various mechanisms, including: physical adsorption, cation exchange, electrostatic interaction, precipitation and complexation (Inyang et al., 2015). Heavy metals immobilized on biochar in soils via these various mechanisms result in different mobility and environmental risks. Physically adsorbed and exchangeable heavy metals on biochar are readily bioavailable and pose immediate risks to the environment (Shen et al., 2017). The stability of the metals immobilized on biochar through electrostatic interaction and precipitation depends on environmental

conditions. For instance, they may be stable in the short term; however, if the environmental conditions change (e.g., significant reduction of soil pH), they may be desorbed/dissolved from the biochar surface and thereby pose risks to the environment (Filgueiras et al., 2002). Complexed metals on biochar are generally regarded as stable and environmentally benign (Filgueiras et al., 2002).

For the reasons discussed above, immobilization mechanisms are very important for biochar application in soil remediation/stabilization. Although some biochars show high adsorption capacities of heavy metals, if the adsorption mechanisms are mainly physical adsorption or cation exchange, these biochars may not be suitable for soil remediation as these weakly bound metals may pose elevated environmental risks in soil. On the other hand, if the immobilization is via precipitation and/or complexation, relatively higher long-term stability is expected compared to physical adsorption and cation exchange.

The mechanisms for biochar removal of heavy metals depend on biochar chemical properties, which is significantly affected by the biochar production process (e.g., production temperature). Although a range of studies have investigated the characteristics and mechanisms of heavy metal adsorption to biochar (Shen et al., 2015; Shen et al., 2017; Shen et al., 2018b), the influence of biochar production temperature on the removal mechanisms remains unclear. It is important to link biochar production temperature and removal mechanisms of heavy metals, for optimal production and application of biochar in soil remediation.

To address this knowledge gap, rice straw biochars were produced at differing temperatures and the effect of production temperature on adsorption characteristics and immobilization mechanisms of lead on the biochars was investigated. Rice straw was selected as a feedstock due to its high availability in China, as one of the most abundant agricultural wastes (Wang et al., 2017), and lead was selected as a representative heavy metal due to its high concentrations in contaminated soils in China (Zhao et al., 2015) and high health risks (especially to children) (Shen et al., 2018a) (O'Connor et al., 2018c). The hypothesis to be verified in this study is that lead retention on the rice straw biochars produced at various temperatures will have different mechanisms, and therefore understanding these differences is critical in producing appropriate biochar for soil remediation.

2 Materials and methods

2.1 Biochar production and characterization

The rice straws used in this study were obtained from Taicang, Suzhou, China. After reception, they were oven dried at 60 °C to reach constant weight. The resulting dried feedstock was then used to produce biochars at 300, 500 and 700 °C (RSB300, RSB500 and RSB700). During production, the rice straw was pyrolyzed in a furnace (under limited air) with a heating rate of 10 °C/min and held at the target terminal temperature for 1 h. After preparation, the biochars were sieved through a #100 mesh sieve (< 0.15 mm) and stored in sealed sample bags.

The pH of the biochars was determined based on the works of Alam et al. (2018 a and

104 b) and von Gunten et al. (2017). Briefly, a certain amount (0.1 g) of biochar was
105 mixed with 10 mL of deionized water and shaken at 250 rpm for 24 h. After
106 centrifugation, the pH of the supernatant was measured. The
107 Brunauer–Emmett–Teller (BET) surface area of the biochar was determined by a
108 Tristar II 3020 (Micromeritics) instrument. The C, H, O, N contents of biochar were
109 tested using a CE-440 Elemental Analyzer (Perkin Elmer).

110 The fundamental vibrations and associated rotational-vibrational structure of the
111 biochars were tested using a VERTEX 70v Fourier-transform infrared spectroscopy
112 (FT-IR) spectrometer (BRUKER) between wavenumbers 4000 to 600 cm^{-1}. The
113 crystalline phases in the biochar were examined using a D8 ADVANCE X-ray
114 diffractometer (XRD) (Bruker). To do so, dry samples were mounted on a flat holder
115 and examined with a Cu Kα source operating at 40 kV and 40 mA, emitting radiation
116 at a wavelength of 1.5406 Å. The scanning regions were between 2θ values of 10-60°
117 at a step rate of 0.1 s/step and a resolution of 0.01°/step. The surface morphology of
118 the biochars (coated with Pt) was tested using a SU8010 Ultra-High Resolution (1.0
119 nm) Scanning Electron Microscope (SEM) (Hitachi, Japan).

120 2.2 Adsorption tests

121 Batch adsorption tests were carried out to reveal the characteristics of Pb adsorption
122 on the rice straw biochars. In order to assess the adsorption kinetics, a certain amount
123 of biochar (0.1 g) was added to 20 mL solution of 5 mM $Pb(NO_3)_2$ containing 0.01 M
124 $NaNO_3$ (for a relatively stable solution ionic strength) in 50-mL polyethylene tubes.

125 The mixtures were shaken at 250 rpm for 5 min, 10 min, 20 min, 30 min, 1 h, 2 h, 3 h,
126 6 h, 12 h, 18 h or 24 h in a temperature-controlled shaker (SHA-CA, Kexi Instrument
127 CO., Ltd.). After the designated shaking time, a mixture was filtered through a 0.45 μm
128 membrane. The Pb concentration in the collected filtrate was measured by inductively
129 coupled plasma/optical emission spectrometry (ICP-OES) (Perkin-Elmer, Optima
130 8300) after dilution (if necessary) and acidification. The kinetics tests confirmed that
131 the equilibrium adsorption time for all biochars was less than 24 hours.

132 In order to construct a sorption isotherm for each biochar, 0.1 g of biochar was added
133 to 20 mL solutions containing different Pb concentrations (0.1, 0.2, 0.3, 0.5, 1, 2, 3, 5,
134 10 or 20 mM) and 0.01 M $NaNO_3$. The mixture was shaken at 200 rpm for 24 h to
135 reach equilibrium before filtration and ICP-OES testing as described above.

136 Pseudo first order, pseudo second order and intraparticle diffusion models are three of
137 the most commonly used kinetics models to reveal the time-dependence of
138 adsorption (Cui et al., 2016; Inyang et al., 2011), and were used to simulate the
139 kinetics data:

140 $$q_t = q_e(1 - e^{-k_1 t}) \quad (1)$$

141 $$q_t = \frac{k_2 {q_e}^2 t}{1 + k_2 q_e t} \quad (2)$$

142 $$q_t = k_i t^{0.5} + C \quad (3)$$

143 where k_1 (h^{-1}) is the rate constant of pseudo first order adsorption, k_2 (g/mg h) is the
144 pseudo second order rate constant, and k_i (mg/g $h^{-0.5}$) is the coefficient of intraparticle
145 diffusion. In equation (2), q_e (mg/g) is the equilibrium adsorption capacity, and q_t (mg/g)

146 in each equation is the adsorbed Pb at time t.

147 Langmuir and Freundlich models are two of the most commonly used isotherm
148 models and were used to describe the equilibrium sorption data (Foo and Hameed,
149 2010):

150 $$q_e = \frac{Q_{max} b C_e}{1 + b C_e} \quad (4)$$

151 $$q_e = K_f {C_e}^{1/n} \quad (5)$$

152 where Q_{max} (mg/g) is the maximum monolayer adsorption capacity, b is the Langmuir
153 isotherm constant (L/mg), K_f (mg/g) is the Freundlich isotherm constant, n represents
154 the adsorption intensity, q_e is the adsorbed Pb (mg/g) at equilibrium and C_e (mg/L) is
155 the equilibrium Pb concentration in solution.

156 2.3 Mechanistic analysis

157 The biochar samples after Pb adsorption were tested by FT-IR and XRD to reveal the
158 mineralogical and molecular changes, using the same testing procedure described in
159 section 2.1. In order to investigate the fractions of immobilized Pb on the biochars, a
160 simplified sequential extraction test was carried out (Shen et al., 2017): (1)
161 approximately 0.1 g solid sample was extracted with 8 mL of 0.5 M $MgCl_2$ (adjust to
162 pH 7.0 using NaOH or HCl) and shaken for 20 min at room temperature; (2) another
163 0.1 g solid sample was extracted with 8 mL of 1 M NaOAc (adjusted to pH 5.0 with
164 HOAc) and shaken for 5 h at room temperature. After shaking, the mixtures were
165 centrifuged and the supernatants collected and filtered through 0.45 μm membranes,
166 and then tested for Pb concentrations by ICP-OES test after dilution (if necessary)

and acidification. The exchangeable Pb on biochar can be calculated from extraction (1); the exchangeable + acid soluble Pb on biochar can be calculated from extraction (2), and therefore the acid soluble Pb can be obtained by subtracting (1) from (2) (Shen et al., 2017). The stable Pb on biochar can be calculated by subtracting the exchangeable and acid soluble Pb from the total adsorbed Pb (obtained from the adsorption studies).

2.4 Statistical analysis

The pH, adsorption and sequential extraction tests were conducted in duplicates, and the mean and standard deviation was reported for each experiment. The micro-structural and other tests were conducted once, and so no statistical analysis appears for these measurements.

3 Results and discussion

3.1 Biochar characterization

Table 1 Characteristics of the rice straw biochars

	RSB300	RSB500	RSB700
Yield	38%	31%	30%
pH	7.89 ± 0.01	10.40 ± 0.01	10.68 ± 0.01
BET surface area (m^2/g)	6.766	22.383	115.465
Average pore size (nm)	14.273	9.576	3.585

C (%)	44.66 ± 0.14	44.53 ± 0.36	44.91 ± 0.75
H (%)	3.06 ± 0.01	1.88 ± 0.01	1.24 ± 0.01
N (%)	1.62 ± 0.02	1.35 ± 0.02	1.03 ± 0.02
O (%)	19.29 ± 0.53	9.75 ± 0.25	5.91 ± 0.24
H:C	0.07	0.04	0.03
O:C	0.43	0.22	0.13

Biochar properties are shown in Table 1. Biochar yield decreases as production temperature increases, however the decreases diminished at high temperatures (from 500 to 700 °C), because most of the volatile components had been removed at lower temperatures (Zhao et al., 2017). RSB300 is slightly alkaline with a pH of 7.89. In comparison, higher production temperature for RSB500 and RSB700 results in much higher pH values (10.40 and 10.68), because higher production temperature leads to the decomposition of acidic functional groups (e.g., carboxyl and phenol) of biochar and the formation of alkaline minerals (e.g., K_2O) (Dodson, 2011). The carbon content of the three biochars were all near 45%. In contrast, H, N, and O contents in the biochars all decreased with increasing production temperature due to the loss of the volatile component and dehydration of organic compounds (Zhao et al., 2017). Correspondingly, H:C and O:C of the biochars decreased with increasing production temperature, suggesting the surface of the biochars were more aromatic and less hydrophilic (Zhao et al., 2017).

The BET surface area of the rice straw biochars was also significantly affected by production temperature. The surface area of RSB300 (6.766 m^2/g) was relatively low, however, it climbs to 22.383 for RSB500 and dramatically increases to 115.465 m^2/g for RSB700. The increased surface area suggests that pores in biochar gradually developed with increased production temperature in 300-700°C, which was also observed in previous studies (Keiluweit et al., 2010; Yang et al., 2015). The increase in surface area from 300 to 500 °C was due to the degradation and destruction of cellulose, which results in the formation of amorphous carbon structure and micropores (Chen et al., 2012; Zhao et al., 2017). The dramatic increase in surface area from 500°C to 700°C was due to the decomposition of lignin and quick release of H_2 and CH_4, which generates significant densities of micropores (Chen et al., 2012; Zhao et al., 2017). This can also be revealed by the decrease of the average pore size with increased production temperature, whereby more and more macropores transferred to meso and micro pores (Table 1). SEM results (Figure 1) show the porous structure of the biochars at the micron scale, however, a quantitative comparison of the porous structure is best confirmed by the BET results discussed above.

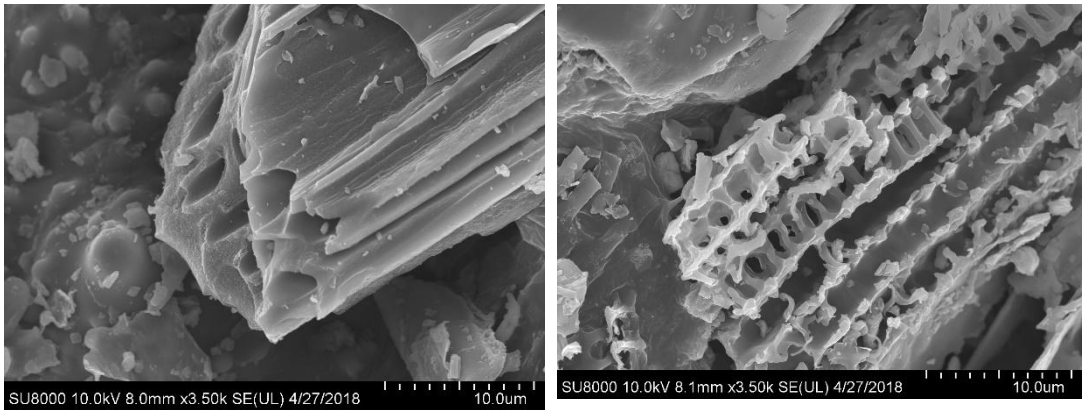

RSB300

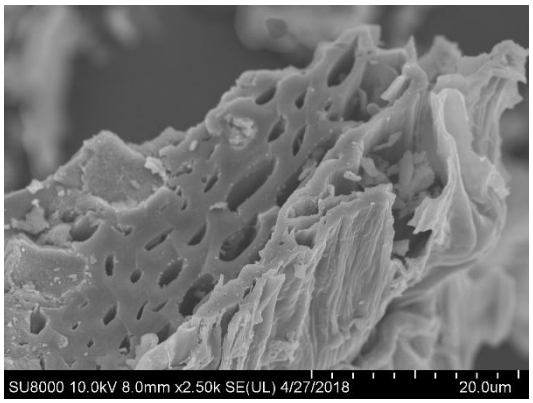

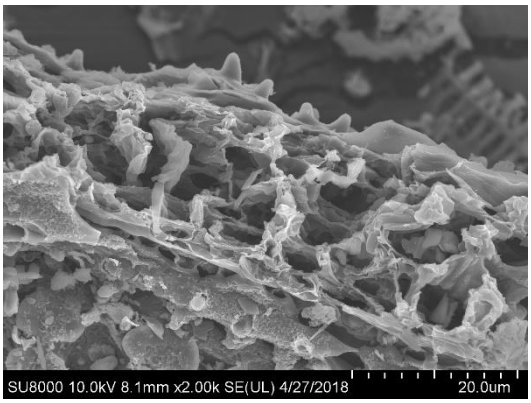

RSB500

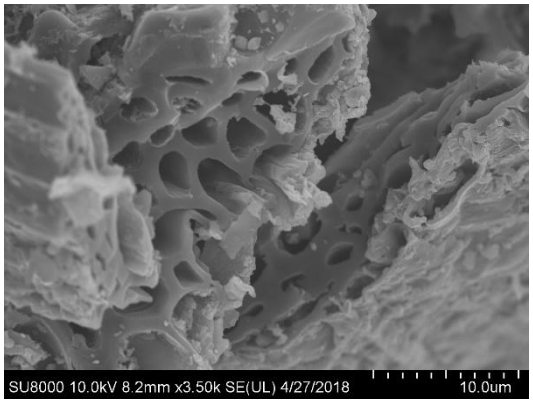

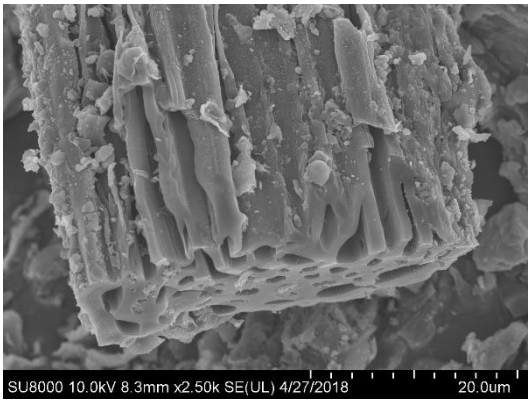

RSB700

212 Figure 1 Surface morphology of the rice straw biochars at different magnifications and
213 cross sections under SEM (a)RSB300; (b)RSB500 and (c)RSB700

214 The FT-IR spectra of the biochars are shown in Figure 2. The peaks at ~1575 and
215 ~800 cm^{-1} that appear in each spectrum are typically found for biochars, representing
216 aromatic carbon (Keiluweit et al., 2010). The peaks at ~1080 cm^{-1} are attributable to
217 the stretching of C-O bonds (Wang et al., 2017). A range of peaks (O-H, C=O and C-H)
218 between 1440-1300 cm^{-1} were observed for RSB300, which originate from the
219 cellulose, hemicellose and lignin (Keiluweit et al., 2010). With higher production

220 temperature, these raw materials decomposed and a more active aromatic structure
221 formed, resulting in the disappearance of the peaks between 1440-1300 cm^{-1} and the
222 appearance of peaks representing aromatic C=C stretching (1414 cm^{-1}) for RSB500
223 (Keiluweit et al., 2010; Wu et al., 2012). At a production temperature of 700 °C, the
224 C=C stretching peak declined due to the progressive condensation of the aromatic
225 structure at high temperatures (Keiluweit et al., 2010; Wu et al., 2012). The XRD
226 patterns are shown in Figure 3, and indicate that the biochars are highly amorphous
227 and contain only KCl as the crystalline phase, which is in line with previous findings on
228 rice straw biochars (Qian et al., 2016; Tan et al., 2017).

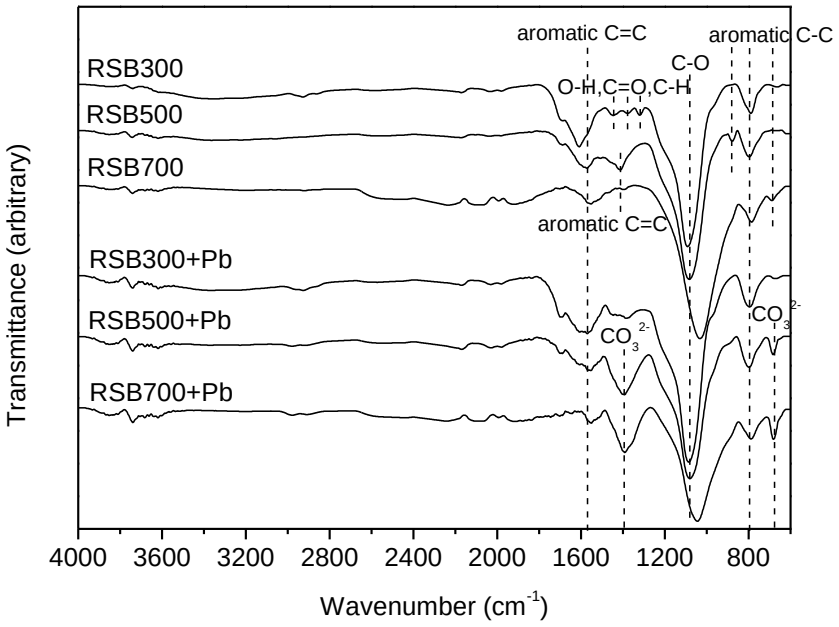

229

230 Figure 2 FT-IR spectra of the rice straw biochars before and after lead adsorption

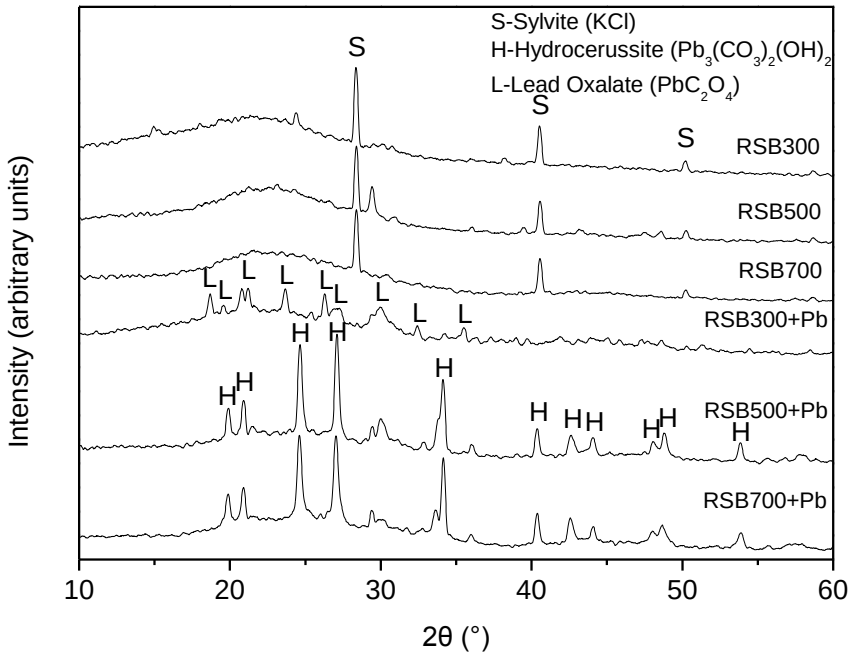

231

232 Figure 3 XRD patterns of the rice straw biochars before and after lead adsorption

233 3.2 Adsorption kinetics and isotherms

234 The adsorption kinetics of lead on the rice straw biochars are shown in Figure 4 and
235 Table 2. The kinetics data were better described using a pseudo second order model
236 (R^2 of 0.88-0.97), which was originally created to describe the kinetics of heavy metal
237 removal by zeolites (Blanchard et al., 1984), as compared with a pseudo first order
238 model (R^2 of 0.71-0.95) for all three biochars. The adsorption capacity (q_e) and k_2
239 values obtained from the pseudo second order model were both in the order of
240 RSB700>RSB500>RSB300. This suggests that higher production temperature can
241 both aid in higher Pb adsorption capacity and faster adsorption kinetics (Plazinski et
242 al., 2009). Nearly all of the Pb (94%) was removed by RSB700 within 1 h. In

243 comparison, RSB500 and RSB300 only removed 73% and 65% of the total Pb at 1 h,

244 respectively, and required 6 h to reach >90% total Pb removal from solution.

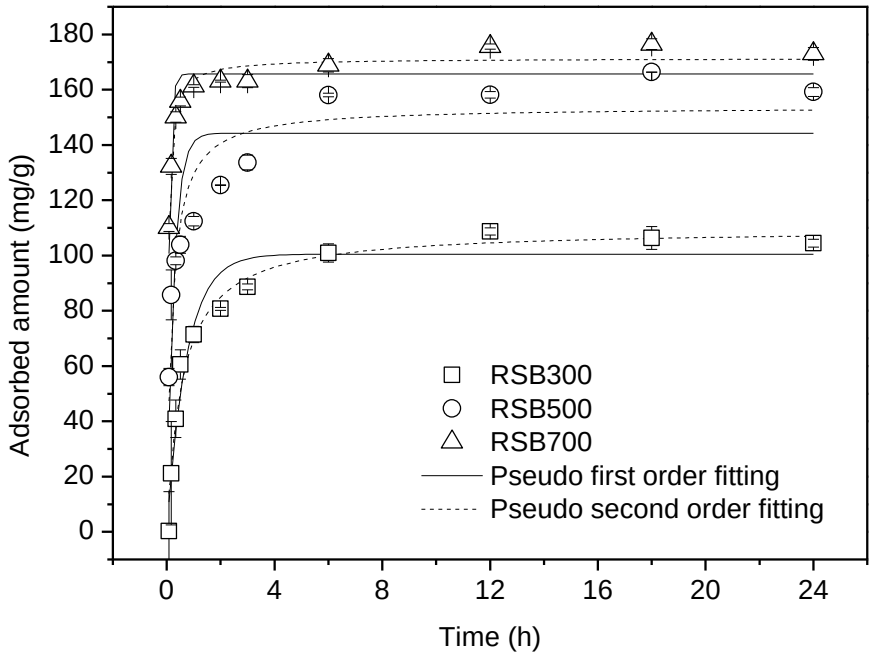

245

246 Figure 4 Adsorption kinetics of lead on rice straw biochars (0.1 g biochar in 20 mL of

247 5mM Pb solution)

248 Table 2 Kinetics parameters for lead adsorption to the rice straw biochars (0.1 g

249 biochar in 20 mL of 5mM Pb solution).

Biochar	Pseudo first order			Pseudo second order		
	q_e (mg/g)	k_1 (h^{-1})	R^2	q_e (mg/g)	k_2 (g/mg h)	R^2
RSB300	100.50±3.76[a]	1.36±0.21	0.95	109.59±3.42	0.02±0.003	0.97
RSB500	144.25±7.42	3.82±0.93	0.71	153.81±5.46	0.03±0.008	0.88

RSB700	165.68±2.98	11.22±1.35	0.81	171.34±1.41	0.12±0.01	0.97

(a – mean ± standard error)

The kinetics were further analyzed by intraparticle plotting (Figure 5 and Table S1). The three biochars exhibit the same three stages of adsorption. The first fast stage is due to the movement of Pb across the external liquid film boundary layer to the external surface sites of biochars (Choy et al., 2004). The second, slower stage is attributed to the migration of Pb within the pores of the biochars by intraparticle diffusion (Choy et al., 2004). The third stage, which appears nearly flat, occurs because the final stage of Pb adsorption was at internal surface sites, which is rapid (Choy et al., 2004). Equilibrium sorption was complete by approximately 6 h, and therefore remained unchanged from 6 to 24 h. The majority of total adsorbed Pb had been adsorbed on RSB700 after the first stage. This was because RSB700 has the largest surface area (Table 1) amongst the three biochars, and therefore has the most accessible surface sites to seat the Pb ions. The data additionally indicate that intraparticle diffusion is the main rate-limiting step for lead adsorption on all the three biochars.

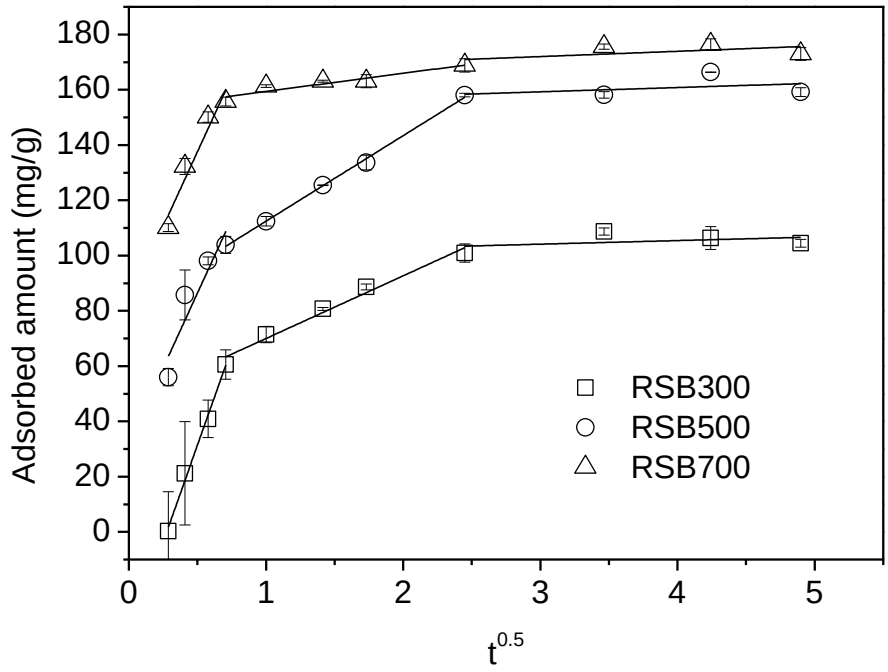

Figure 5 Plots of intraparticle diffusion for lead adsorption on the rice straw biochars

The adsorption isotherms are shown in Figure 6 (equilibrium pH shown in Table S2). The Langmuir model generally shows better goodness of fitness for the equilibrium data, except RSB700, for which Freundlich resulted in a slightly better fit. The calculated maximum monolayer adsorption capacities for RSB300, RSB500 and RSB700 were 100.27, 164.62 and 198.18 mg/g respectively. This finding was in line with the kinetics findings that the rice straw biochars with higher production temperatures tend to have higher Pb adsorption capacities. The observed maximum monolayer adsorption capacities of the rice straw biochars in this study were higher than most of the reported adsorption capacities of biochars reported in existing literature (Inyang et al., 2015; Li et al., 2017), suggesting that rice straw is a promising biochar feedstock for heavy metal adsorption.

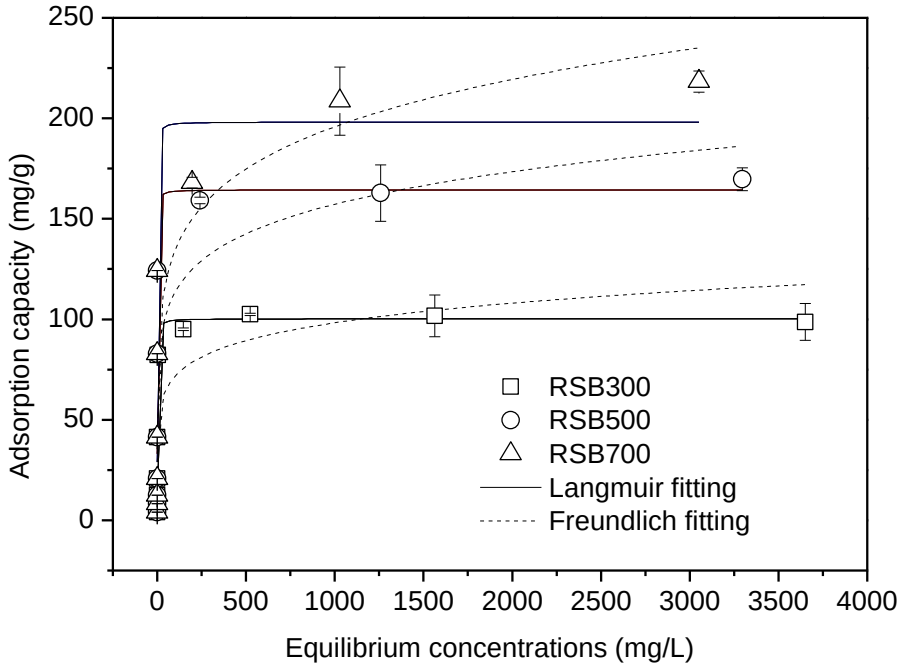

278

279 Figure 6 Adsorption isotherms of lead on rice straw biochars (0.1 g biochar in 20 mL

280 solution)

281 Table 3 Parameters for Langmuir and Freundlich modelling (0.1 g biochar in 20 mL

282 solution)

Biochar	Langmuir			Freundlich		
	Q_{max} (mg/g)	b (L/mg)	R^2	K_f (mg/g)	1/n	R^2
RSB300	100.27±2.88[a]	1.30±0.22	0.98	38.18±8.65	0.14	0.74
RSB500	164.62±21.81	2.26±1.10	0.71	59.15±15.66	0.14	0.65
RSB700	198.18±25.40	1.96±1.08	0.73	63.13±6.10	0.16	0.77

283 (a – mean ± standard error)

3.3 Adsorption mechanisms

After batch adsorption experiments, the rice straw biochars were tested by XRD, FT-IR and sequential extractions to investigate the immobilization mechanisms. The XRD results (Figure 3) show that lead oxalate (PbC_2O_4) was formed on RSB300, whereas hydrocerussite ($Pb_3(CO_3)_2(OH)_2$) was formed on RSB500 and RSB700. Low-temperature rice straw biochars (100-300 °C) favor the formation of calcium oxalate (CaC_2O_4) (Qian et al., 2016). With the increase of production temperature (to 500 and 700 °C), the calcium oxalate decomposes and forms calcite ($CaCO_3$) (Qian et al., 2016). This explains the formation of lead oxalate for RSB300 and hydrocerussite for RSB500 and RSB700 after Pb adsorption. The XRD results generally suggest that precipitation was a mechanism for Pb removal by the rice straw biochars. The FT-IR results (Figure 2) also show the presence of CO_3^{2-} for RSB500 and RSB700 after Pb adsorption, which is likely due to the newly-formed hydrocerussite.

The fractions of Pb immobilized by the biochars are shown in Figure 7 and Figure S1. The stable Pb concentrations on RSB300, RSB500 and RSB700 were 61.50, 91.59 and 99.11 mg/g, accounting for 60.01%, 57.55% and 59.00% of their total Pb loadings, respectively. The acid soluble Pb on RSB300, RSB500 and RSB700 was 29.33, 66.18 and 68.40 mg/g, accounting for 28.62%, 41.58% and 40.72% of their total Pb loadings respectively. These results clearly show that the increased Pb removal capacity by increased production temperature for the rice straw biochars (Table 3) comes from the increased acid soluble and stable Pb. In contrast, the exchangeable Pb significantly decreased for the high-temperature rice straw biochars. RSB300 has 11.64 mg/g

306 exchangeable Pb, accounting for 11.34% of its total immobilized amount, however,
307 RSB500 and RSB700 only have 1.39 and 0.47 mg/g exchangeable Pb, which are
308 0.87% and 0.28% of their total immobilized amount respectively.

309 The higher exchangeable Pb concentration for RSB300 was due to its having more
310 exchangeable cations (H^+, K^+) that exchanged with Pb^{2+}, as compared with RSB500
311 and RSB700. These cations come from carboxylic and phenolic groups on RSB300
312 (Dodson, 2011). With the increase of production temperature, the carboxylic and
313 phenolic groups decompose, and H^+ and K^+ form H_2O and K_2O (Dodson, 2011).
314 Therefore, RSB500 and RSB700 have less exchangeable cations for Pb exchange,
315 but higher pH due to the loss of H^+ and formation of alkaline minerals (e.g., K_2O)
316 (Dodson, 2011). The higher pH of RSB500 and RSB700 thereby aids the formation of
317 hydrocerussite.

318 3.4 Implications for soil remediation

319 Soil contamination by heavy metals is a great environmental concern in China and
320 globally (Hou et al., 2017a). It is important to seek greener and more sustainable
321 technological solutions to address contaminated land (Hou et al., 2017b; O'Connor et
322 al., 2018a). The rationale for biochar application in soil remediation is to immobilize
323 the heavy metals within the soil and thereby reduce environmental risks that result
324 from their presence. As mentioned in the introduction section, biochar can
325 immobilize/adsorb heavy metals through a range of mechanisms, and each
326 mechanism results in different binding strengths and environmental risks in the

context of the soil environment.

In this study, the majority of Pb immobilized by the biochars are generally stable according to sequential leaching results (Filgueiras et al., 2002), suggesting that the majority of Pb on rice straw biochars are of low risk in the context of the soil environment. RSB300 has 11.34% of total immobilized Pb attributing to exchangeable fraction, which is highly mobile and of high risks. Therefore, if applied in soil remediation, a certain amount of immobilized Pb on RSB300 may easily leach to the environment, suggesting that RSB300 may not be as appropriate for Pb decontamination as compared with RSB500 and RSB700, which have very low exchangeable fractions. RSB500 and RSB700 have ~40% of the total immobilized Pb attributed to the acid soluble fraction. This Pb may be stable in the short-term, however, when applied in soil, may pose risks after field ageing (e.g., acidic rain exposure) in the long term.

The XRD results show that a certain amount of lead was precipitated to lead oxalate on RSB300 and hydrocerussite on RSB500 and RSB700. Lead oxalate is slightly soluble (e.g., K_{sp} of 10^{-9}, and 4.5 mg/L Pb^{2+} for saturated solution of lead oxalate in water at 26 °C (Kolthoff et al., 1942)). In addition, higher oxalate concentrations (e.g., ≥ 0.05 M) can significantly dissolve lead oxalate due to complexation (Kolthoff et al., 1942). Lower solution pH (e.g., < 4) can also dramatically dissolve lead oxalate (Sayer et al., 1999). Therefore, lead oxalate is unstable in the soil environmental under aggressive environmental conditions and may pose risks in the long term.

In comparison, hydrocerussite has a much lower solubility (e.g., K_{sp} of 10^{-47}, and ~ 0.08 mg/L Pb^{2+} for saturated solution at 20 °C (Mohammadzadeh et al., 2015)). RSB500 and RSB700 have significantly higher pH values (Table 1) as compared to RSB300, and consequently have much stronger buffering capacities against conditions such as acidic rain in the context of the soil environment. Therefore, RSB500 and RSB700 are more applicable for soil remediation of divalent metals such as Pb.

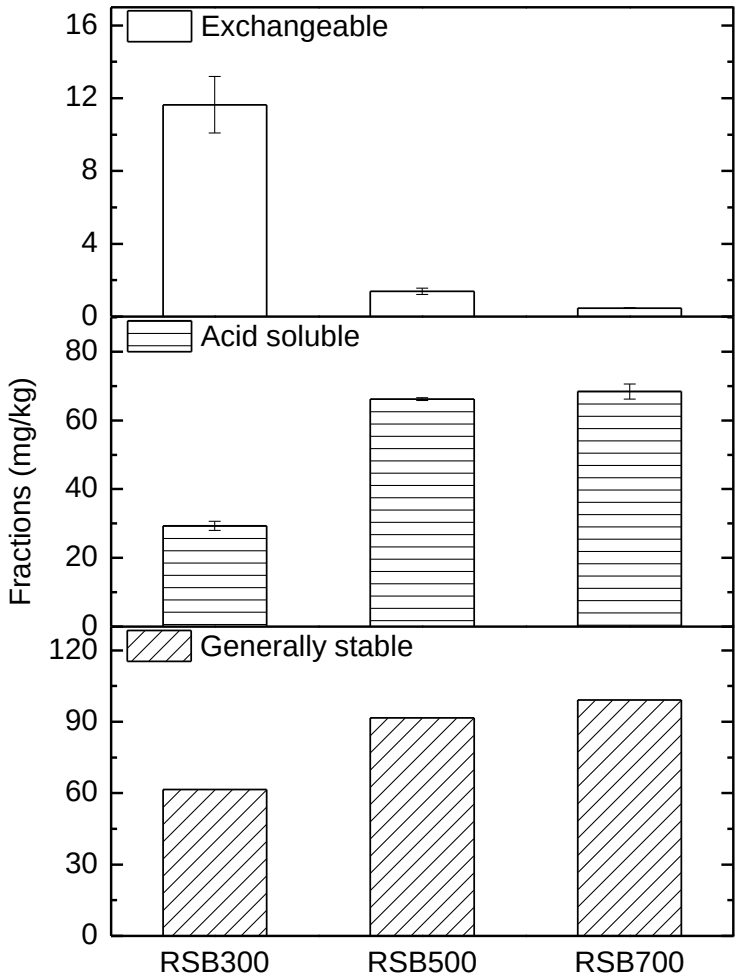

Figure 7 Fractions (mg/mg) of lead adsorbed on the biochars

4 Conclusions

Rice straw biochars were produced at 300, 500 and 700 °C. The influence of production temperature on the adsorption characteristics and mechanisms of lead on rice straw biochars were investigated. Biochars produced at higher temperatures have significant higher pH values and surface areas, resulting in higher Pb removal capacities and faster adsorption kinetics. Precipitation was a mechanism by which all three biochars immobilized Pb: lead oxalate was precipitated on RSB300 and hydrocerussite was precipitated on RSB500 and RSB700. The immobilized lead on the biochars can be divided into exchangeable, acid soluble and non-available fractions. RSB300 has 11.34% of total immobilized Pb attributed to the exchangeable fraction, whereas for RSB500 and RSB700, this fraction was less than 1%. The immobilized Pb on RSB500 and RSB700 is attributable to acid soluble and non-available fractions (>99%). Based on the mechanistic analyses discussed above, RSB500 and RSB700 are much more appropriate for soil remediation as compared with RSB300. Field-scale applications of rice straw biochars for heavy metal stabilization in soil are suggested for future research, to verify the laboratory findings of the present study.

Acknowledgements

This work was supported by the Opening Fund of National Engineering Laboratory for Site Remediation Technologies (No. NEL-SRT201702), and the National Water

377 Pollution Control and Treatment Science and Technology Major Project (No.
378 2018ZX07109-003). Moreover, this study was partly funded by the Thousand Talents
379 Program of the Chinese government and Tsinghua University. The first author would
380 like to thank the Killam Trusts of Canada for kindly providing the Izaak Walton Killam
381 Memorial Postdoctoral Fellowship.

382 References

383 Alam, M.S., Swaren, L., von Gunten, K., Cossio, M., Bishop, B., Robbins, L.J., Hou,
384 D., Flynn, S.L., Ok, Y.S., Konhauser, K.O., Alessi, D.S., 2018a. Application of
385 surface complexation modeling to trace metals uptake by biochar-amended
386 agricultural soils. Appl. Geochemistry 88, 103–112.
387 doi:10.1016/j.apgeochem.2017.08.003

388 Alam, M., Gorman-Lewis, D., Chen, N., Flynn, S.L., Ok, Y., Konhauser, K., Alessi,
389 D.S., 2018b. Thermodynamic Analysis of Nickel (II) and Zinc (II) Adsorption to
390 Biochar. Environ. Sci. Technol. doi:10.1021/acs.est.7b06261

391 Blanchard, G., Maunaye, M., Martin, G., 1984. Removal of heavy metals from waters
392 by means of natural zeolites. Water Res. 18, 1501–1507.

393 Chen, Y., Yang, H., Wang, X., Zhang, S., Chen, H., 2012. Biomass-based pyrolytic
394 polygeneration system on cotton stalk pyrolysis: Influence of temperature.
395 Bioresour. Technol. 107, 411–418. doi:10.1016/j.biortech.2011.10.074

396 Choy, K.K.H., Ko, D.C.K., Cheung, C.W., Porter, J.F., McKay, G., 2004. Film and
397 intraparticle mass transfer during the adsorption of metal ions onto bone char. J.

398 Colloid Interface Sci. 271, 284–295. doi:10.1016/j.jcis.2003.12.015

399 Cui, X., Hao, H., Zhang, C., He, Z., Yang, X., 2016. Science of the Total Environment
400 Capacity and mechanisms of ammonium and cadmium sorption on different
401 wetland-plant derived biochars. Sci. Total Environ. 539, 566–575.
402 doi:10.1016/j.scitotenv.2015.09.022

403 Dodson, J., 2011. Wheat straw ash and its use as a silica source.

404 Filgueiras, a V, Lavilla, I., Bendicho, C., 2002. Chemical sequential extraction for
405 metal partitioning in environmental solid samples. J. Environ. Monit. 4, 823–857.
406 doi:10.1039/b207574c

407 Foo, K.Y., Hameed, B.H., 2010. Insights into the modeling of adsorption isotherm
408 systems. Chem. Eng. J. 156, 2–10. doi:10.1016/j.cej.2009.09.013

409 Gunten, K. Von, Alam, S., Hubmann, M., Sik, Y., Konhauser, K.O., Alessi, D.S., 2017.
410 Bioresource Technology Modified sequential extraction for biochar and
411 petroleum coke : Metal release potential and its environmental implications.
412 Bioresour. Technol. 236, 106–110. doi:10.1016/j.biortech.2017.03.162

413 Hou, D., Al-Tabbaa, A., 2014. Sustainability: A new imperative in contaminated land
414 remediation. Environ. Sci. Policy 39, 25–34. doi:10.1016/j.envsci.2014.02.003

415 Hou, D., Ding, Z., Li, G., Wu, L., Hu, P., Guo, G., Wang, X., Ma, Y., O'Connor, D.,
416 Wang, X., 2017a. A Sustainability Assessment Framework for Agricultural Land
417 Remediation in China. L. Degrad. Dev. doi:10.1002/ldr.2748

418 Hou, D., Li, F., n.d. Complexities Surrounding China's Soil Action Plan. L. Degrad.
419 Dev.

420 Hou, D., O'Connor, D., Nathanail, P., Tian, L., Ma, Y., 2017b. Integrated GIS and
421 multivariate statistical analysis for regional scale assessment of heavy metal soil
422 contamination: A critical review. Environ. Pollut.

423 Inyang, M., Gao, B., Ding, W., Pullammanappallil, P., Zimmerman, A.R., Cao, X.,
424 2011. Enhanced Lead Sorption by Biochar Derived from Anaerobically Digested
425 Sugarcane Bagasse. Sep. Sci. Technol. 46, 1950–1956.
426 doi:10.1080/01496395.2011.584604

427 Inyang, M.I., Gao, B., Yao, Y., Xue, Y., Zimmerman, A., Mosa, A., Pullammanappallil,
428 P., Ok, Y.S., Cao, X., 2015. A Review of Biochar as a Low-Cost Adsorbent for
429 Aqueous Heavy Metal Removal. Crit. Rev. Environ. Sci. Technol. 00–00.
430 doi:10.1080/10643389.2015.1096880

431 Keiluweit, M., Nico, P.S., Johnson, M., Kleber, M., 2010. Dynamic molecular structure
432 of plant biomass-derived black carbon (biochar). Environ. Sci. Technol. 44,
433 1247–1253. doi:10.1021/es9031419

434 Kolthoff, I.M., Perlich, R.W., Weiblen, D., 1942. The solubility of lead sulfate and of
435 lead oxalate in various media. J. Phys. Chem. 46, 561–570.
436 doi:10.1021/j150419a004

437 Li, H., Dong, X., da Silva, E.B., de Oliveira, L.M., Chen, Y., Ma, L.Q., 2017.
438 Mechanisms of metal sorption by biochars: Biochar characteristics and

439 modifications. Chemosphere 178, 466–478.
440 doi:10.1016/j.chemosphere.2017.03.072

441 Mohammadzadeh, M., Basu, O.D., Herrera, J.E., 2015. Impact of Water Chemistry on
442 Lead Carbonate Dissolution in Drinking Water Distribution Systems 389–397.

443 O'Connor, D., Hou, D., Ok, Y.S., Song, Y., Sarmah, A., Li, X., Tack, F.M.G., 2018a.
444 Sustainable in situ remediation of recalcitrant organic pollutants in groundwater
445 with controlled release materials: A review. J. Control. Release.

446 O'Connor, D., Peng, T., Zhang, J., Tsang, D.C.W., Alessi, D.S., Shen, Z., Bolan, N.S.,
447 Hou, D., 2018b. Biochar application for the remediation of heavy metal polluted
448 land: A review of in situ field trials. Sci. Total Environ. 619–620, 815–826.
449 doi:10.1016/j.scitotenv.2017.11.132

450 O'Connor D, Hou D, Ye J, Zhang Y, Ok YS, Song Y, et al. Lead-based paint remains a
451 major public health concern: A critical review of global production, trade, use,
452 exposure, health risk, and implications. Environment international 2018c; 121:
453 85-101.

454 Plazinski, W., Rudzinski, W., Plazinska, A., 2009. Theoretical models of sorption
455 kinetics including a surface reaction mechanism: A review. Adv. Colloid Interface
456 Sci. 152, 2–13. doi:10.1016/j.cis.2009.07.009

457 Qian, L., Zhang, W., Yan, J., Han, L., Gao, W., Liu, R., Chen, M., 2016. Bioresource
458 Technology Effective removal of heavy metal by biochar colloids under different
459 pyrolysis temperatures. Bioresour. Technol. 206, 217–224.

doi:10.1016/j.biortech.2016.01.065

Alam, M., Gorman-Lewis, D., Chen, N., Flynn, S.L., Ok, Y., Konhauser, K., Alessi, D.S., 2018. Thermodynamic Analysis of Nickel (II) and Zinc (II) Adsorption to Biochar. Environ. Sci. Technol. doi:10.1021/acs.est.7b06261

Sayer, J.A., Cotter-Howells, J.D., Watson, C., Millier, S., Gadd, G.M., 1999. Lead mineral transformation by fungi. Curr. Biol. 9, 691–694. doi:10.1016/S0960-9822(99)80309-1

Shen, Z., Hou, D., Zhang, P., Wang, Y., Zhang, Y., Shi, P., O'Connor, D., 2018a. Lead-based paint in children's toys sold on China's major online shopping platforms. Environ. Pollut. 241. doi:10.1016/j.envpol.2018.05.078

Shen, Z., Jin, F., Wang, F., McMillan, O., Al-Tabbaa, A., 2015. Sorption of lead by Salisbury biochar produced from British broadleaf hardwood. Bioresour. Technol. 193, 553–556. doi:10.1016/j.biortech.2015.06.111

Shen, Z., Zhang, Y., Jin, F., Alessi, D.S., Zhang, Y., Wang, F., McMillan, O., Al-Tabbaa, A., 2018b. Comparison of nickel adsorption on biochars produced from mixed softwood and Miscanthus straw. Environ. Sci. Pollut. Res. doi:10.1007/s11356-018-1674-2

Shen, Z., Zhang, Y., Jin, F., Mcmillan, O., Al-tabbaa, A., 2017. Science of the Total Environment Qualitative and quantitative characterisation of adsorption mechanisms of lead on four biochars. Sci. Total Environ. 609, 1401–1410. doi:10.1016/j.scitotenv.2017.08.008

481 Shen, Z., Zhang, Y., McMillan, O., Jin, F., Al-Tabbaa, A., 2017. Characteristics and
482 mechanisms of nickel adsorption on biochars produced from wheat straw pellets
483 and rice husk. Environ. Sci. Pollut. Res. 24. doi:10.1007/s11356-017-8847-2

484 Sohi, S.P., 2012. Agriculture. Carbon storage with benefits. Science 338, 1034–5.
485 doi:10.1126/science.1225987

486 Tan, Z., Wang, Y., Kasiulienė, A., Huang, C., Ai, P., 2017. Cadmium removal potential
487 by rice straw-derived magnetic biochar. Clean Technol. Environ. Policy 19,
488 761–774. doi:10.1007/s10098-016-1264-2

489 Wang, H., Chu, Y., Fang, C., Huang, F., Song, Y., Xue, X., 2017. Sorption of
490 tetracycline on biochar derived from rice straw under different temperatures.
491 PLoS One 12, 1–14. doi:10.1371/journal.pone.0182776

492 Wang, X., Liu, N., Liu, Y., Jiang, L., Zeng, G., Tan, X., Liu, S., Yin, Z., Tian, S., Li, J.,
493 2017. Adsorption removal of 17β-estradiol from water by rice straw-derived
494 biochar with special attention to pyrolysis temperature and background chemistry.
495 Int. J. Environ. Res. Public Health 14, 1–17. doi:10.3390/ijerph14101213

496 Wu, W., Yang, M., Feng, Q., McGrouther, K., Wang, H., Lu, H., Chen, Y., 2012.
497 Chemical characterization of rice straw-derived biochar for soil amendment.
498 Biomass and Bioenergy 47, 268–276. doi:10.1016/j.biombioe.2012.09.034

499 Yang, G.. b, Wang, Z.., Xian, Q.., Shen, F.., Sun, C.., Zhang, Y.., Wu, J.., 2015.
500 Effects of pyrolysis temperature on the physicochemical properties of biochar
501 derived from vermicompost and its potential use as an environmental

amendment. RSC Adv. 5, 40117–40125. doi:10.1039/c5ra02836a

Zhao, B., O'Connor, D., Zhang, J., Peng, T., Shen, Z., Tsang, D.C.W., Hou, D., 2017. Effect of pyrolysis temperature, heating rate, and residence time on rapeseed stem derived biochar. J. Clean. Prod. 174, 977–987. doi:10.1016/j.jclepro.2017.11.013

Zhao, F.J., Ma, Y., Zhu, Y.G., Tang, Z., McGrath, S.P., 2015. Soil contamination in China: Current status and mitigation strategies. Environ. Sci. Technol. 49, 750–759. doi:10.1021/es5047099

Zhao, S.X., Ta, N., Wang, X.D., 2017. Effect of temperature on the structural and physicochemical properties of biochar with apple tree branches as feedstock material. Energies 10. doi:10.3390/en10091293

Supplementary material for on-line publication only

Click here to download Supplementary material for on-line publication only: Supporting Information.docx